Supplemental Information

Photo-steered rapid and multimodal locomotion of 3D-printed tough hydrogel robots

Min Dong[a], Weixuan Liu[b], Chen Fei Dai[a], Dejin Jiao[a], Qing Li Zhu[a], Wei Hong[b], Jun Yin[c], Qiang Zheng[a] and Zi Liang Wu[a,*]

[a] Ministry of Education Key Laboratory of Macromolecular Synthesis and Functionalization
Department of Polymer Science and Engineering
Zhejiang University
Hangzhou 310058, China

[b] Shenzhen Key Laboratory of Soft Mechanics & Smart Manufacturing
Department of Mechanics and Aerospace Engineering
Southern University of Science and Technology
Shenzhen 518055, China

[c] The State Key Laboratory of Fluid Power and Mechatronic Systems
Key Laboratory of 3D Printing Process and Equipment of Zhejiang Province
School of Mechanical Engineering
Zhejiang University
Hangzhou 310058, China

* Corresponding author. E-mail: wuziliang@zju.edu.cn

Experimental Section

Materials

Cetyltrimethylammonium bromide (CTAB), gold (III) chloride trihydrate ($HAuCl_4 \cdot 3H_2O$), silver nitrate ($AgNO_3$), and sodium borohydride ($NaBH_4$) were purchased from Sigma-Aldrich. *N*-isopropylacrylamide (NIPAm) was purchased from Tokyo Chemical Industry (Shanghai) Development Co., Ltd. Acrylic acid (AAc), acrylamide (AAm), potassium persulfate (KPS), *N*,*N*,*N*′,*N*′-tetramethylethylenediamine (TEMED), and zirconyl chloride octahydrate ($ZrOCl_2 \cdot 8H_2O$) were used as received from Aladdin Chemistry Co., Ltd. Ascorbic acid was received from Sinopharm Chemical Reagent Co., Ltd. Methoxy polyethylene glycol thiol (MPEG-SH; weight-average molecular weight, M_w = 5,000) was purchased from Beijing Jenkem Technology Co., Ltd. Millipore deionized water (18.2 MΩ/cm) was used in all the experiments.

Synthesis and PEGylation of Gold Nanorods

AuNRs were prepared by a seed-mediated method reported in the literature.[1, 2] The seed solution was synthesized by quick addition of a fresh, ice-cold aqueous solution of $NaBH_4$ (500 μL, 0.01 M) into an aqueous mixture solution of CTAB (3.50 mL, 0.2 M) and $HAuCl_4$ (125 μL, 0.015 M) at 25.5 °C. After stirring vigorously for 2 min, the resultant brownish yellow solution was kept in a water bath of 25.5 °C, thus obtained seed solution can be used within 2 h. The growth solution was obtained by adding a newly prepared aqueous solution of ascorbic acid (124 μL, 0.08 M) into the mixture solution of $HAuCl_4$ (520 μL, 0.015 M), $AgNO_3$ (400 μL, 0.004 M), and CTAB (8.82 mL, 0.2 M). The seed solution (100 μL) was quickly added to the growth solution after it became colorless from dark orange. The obtained solution was placed in a 27 °C water bath for 12 h to produce AuNRs. The concentration of AuNRs was evaluated to be 1 nM. To achieve PEGylation of AuNRs, the prepared suspension of AuNRs was centrifuged to remove the extra CTAB, and then the concentrated solution was dispersed in an isometric aqueous solution of MPEG-SH (1 mg/mL). The solution can be used after being placed at room temperature overnight without disturbance.

Synthesis of Copolymers as Inks

The highly viscoelastic inks were facilely prepared by polymerization of the aqueous precursor

solutions. The aqueous solutions of P(AAc-*co*-AAm) and P(AAc-*co*-NIPAm) with different concentrations of AuNRs were synthesized by free-radical copolymerization of monomers.[3] The recipes of the precursor solutions are listed in Table S2. After degassing for 20 min by bubbling of argon gas, the accelerator TEMED was added to the precursor solution, which was transferred into a reaction cell and kept at room temperature for 48 h to complete the polymerization. Highly viscous liquids of P(AAc-*co*-AAm) and P(AAc-*co*-NIPAm) were obtained. The highly viscous liquids of P(AAc-*co*-AAm) and P(AAc-*co*-NIPAm) was directly used as passive and active layers' ink, respectively. The printing ink for transition layer by mixing highly viscous liquids of P(AAc-*co*-AAm) and P(AAc-*co*-NIPAm) with a volume ratio of 50% each. The recipes of printing ink for passive, transition and active layers are listed in Table S3.

3D Printing of Tough Hydrogels

The customized 3D printing system was composed of an extrusion system and a 3D positioning stage. The extrusion system consisted of an air pump, a pressure controller, and a multi-nozzle print head. The viscous copolymer solutions were extruded out of the nozzle at room temperature onto a glass substrate at room temperature and were immediately transferred into 0.1 M $ZrOCl_2$ aqueous solution for gelation and toughening of the printed constructs. Robust gel fibers or printed constructs were incubated in large amount of water at room temperature for 12 h to remove the residuals and achieve the equilibrium state. Detailed printing parameters are listed in Table S3.

Characterizations

Transmission electron microscope (TEM) images of AuNRs were obtained by using a JEOL JEM·1010 electron microscope. Absorption spectra of the aqueous suspensions of AuNRs were measured using a UV-1800 spectrometer (Shimadzu Corp., Japan). The suspensions were kept in a quartz cuvette with an optical path of 1/3 cm for the measurement at room temperature. To monitor the photothermal effect of the AuNRs within the printed gels, the localized temperature of the gel under irradiation of 808 nm NIR light was monitored using an infrared imager (FLIR E60).

Rheological behaviors of the copolymer solutions were characterized by using ARG-2 rheometer (TA Instruments, USA) with plane plate (diameter, 40 mm). Steady shear measurements were performed to the solutions at room temperature with the shear rate varying from 0.01 to 100 s^{-1}.

Tensile tests of single gel fibers were performed by using a commercial tensile tester (Instron 3343) to characterize the mechanical properties of gel fibers and the bonding strength between the gel fibers. The tests were carried out at room temperature with a stretch rate of 100 mm min^{-1}. The nominal stress and strain were recorded, and the Young's modulus was calculated from the slope of the stress-strain curve with a strain below 10%. The tensile breaking stress and breaking strain were extracted from the stress-strain curve for at least three separate tests. To characterize the interfacial bonding between different gels, two fibers were printed into a cross structure. Two ends of the stacked gel were clamped on the tensile tester and stretched at room temperature with a constant rate of 100 mm/min. The force and displacement were recorded. Since the bonding area between gel fibers was difficult to measure, the interfacial bonding was characterized by the apparent strength, as calculated by the facture force divided by the initial cross-section area of the gel fiber. Swelling ratio, S, of the printed gel is examined by measuring the length of the gel fiber, $S = l / l_0$, in which l_0 and l are the length of gel fiber before and after the soaking and toughening process. Water content of the hydrogel, q, was calculated by $q = (w_s\text{-}w_d)/w_s$, where w_s and w_d are the mass of gel in swollen and dried states, respectively.

Numerical Simulations

The actuation of the hydrogel robots is mainly due to the highly anisotropic texture with specific orientations in the printed layers. To further unveil the detailed mechanism, we model the motions of the modular gel robot by solving the equations of mechanical equilibrium with frictional contact and thermal radiation, with the aid of the commercial finite element package COMSOL Multiphysics 5.4.

For simplicity, without resolving individual printed strand, we model each layer as a homogenous and orthotropic material, possessing zero Poisson's ratio and negligible modulus in the transverse direction. The volume-transition-induced deformation is modeled by introducing an inelastic strain

$$\epsilon^{(i)} = \epsilon_t e_{\parallel} \otimes e_{\parallel}, \#(1)$$

where $e_{\parallel}$ is the unit vector parallel to the printed hydrogel strands and $\otimes$ denotes a tensor product. The magnitude of inelastic strain, ϵ_t, is taken to be a function of the normalized temperature T. Both $e_{\parallel}$ amd ϵ_t take different values in distinct layers. The total strain ϵ is then written as the sum of the

elastic and inelastic strains as

$$\epsilon = \epsilon^{(e)} + \epsilon^{(i)}. \#(2)$$

As the motion of the gels is relatively slow, all inertial effects are neglected except for the gravity, which is necessary in the frictional contact between the gel robot and the supporting surface. The frictional contact is modeled by applying a penalty contact force in the normal direction

$$f_n = \begin{cases} -d\exp(-d), & d < 0 \\ 0, & d \geq 0 \end{cases} \#(3)$$

and a friction force tangential to the surface of contact

$$f_t = -\eta f_n \frac{v}{|v|}, \#(4)$$

where d is the normal distance between surfaces, v is the relative sliding velocity, and η is the friction coefficient.

In a typical actuation process, the region under the laser beam is heated locally with a minor effect of thermal conduction. Neglecting thermal conduction, we model the temperature evolution by solving a modified Stefan–Boltzmann equation

$$\frac{\partial T(X,t)}{\partial t} = r(x(X),t) - \beta T(X,t) \#(5)$$

where $r(x,t)$ characterizes the heating intensity of the laser beam, depending on the current (deformed) position x, and β is a parameter characterizing the emissivity of the gel to the environment. The parameters are obtained by fitting the dynamic response of the gel fibers.

References

S1 C. F. Dai, C. Du, Y. Xue, X. N. Zhang, S. Y. Zheng, K. Liu, Z. L. Wu and Q. Zheng, *ACS Appl. Mater. Interfaces*, 2019, **11**, 43631-43640.

S2 G. Cheng, D. Xu, Z. Lu and K. Liu, *ACS Nano*, 2019, **13**, 1479-1489.

S3 S. Y. Zheng, Y. Shen, F. Zhu, J. Yin, J. Qian, J. Fu, Z. L. Wu and Q. Zheng, *Adv. Funct. Mater.*, 2018, **28**, 1803366.

Table S1 Robotic performances of various hydrogel-based soft robots with different elastic moduli upon cyclic heating or light irradiation.

System	Motion mode	Motion speed	Modulus	Ref.
Anisotropic PNIPAm gel	Walking	3.7×10^{-1} mm/s	6 kPa	S4
Anisotropic PNIPAm gel	Walking	3.7×10^{-2} mm/s	10 kPa	S5
Anisotropic PNIPAm gel	Walking	1.5×10^{-1} mm/s	8 kPa	S10
Sponge-like PNIPAm gel	Walking	9.0×10^{-2} mm/s	30 kPa	S11
PNIPAm gel	Walking	6.7×10^{-3} mm/s	10 kPa	S13
PNIPAm gel	Walking	3.8×10^{-3} mm/s	10 kPa	S6
PNIPAm gel	Walking	1.9×10^{-3} mm/s	15 kPa	S12
Spirogyran-containing gel	Walking	8.0×10^{-3} mm/s	10 kPa	S7
Spirogyran-containing gel	Walking	2.5×10^{-4} mm/s	5 kPa	S9
Spirogyran-containing gel	Walking	6.6×10^{-5} mm/s	10 kPa	S8
Printed tough gel	Walking	4.03×10^{-1} mm/s	490-3290 kPa	This work
Anisotropic PNIPAm gel	Turning	9.4×10^{-3} rad/s	6 kPa	S4
Sponge-like PNIPAm gel	Turning	1×10^{-2} rad/s	30 kPa	S11
Spirogyran-containing gel	Turning	4.6×10^{-4} rad/s	10 kPa	S8
Printed tough gel	Turning	3.5×10^{-3} rad/s	490-3290 kPa	This work

S4 Q. L. Zhu, C. Du, Y. Dai, M. Daab, M. Matejdes, J. Breu, W. Hong, Q. Zheng and Z. L. Wu, *Nat. Commun.*, 2020, **11**, 5166.

S5 Y. S. Kim, M. Liu, Y. Ishida, Y. Ebina, M. Osada, T. Sasaki, T. Hikima, M. Takata and T. Aida, *Nat. Mater.*, 2015, **14**, 1002-1007.

S6 S. Maeda, Y. Hara, T. Sakai, R. Yoshida and S. Hashimoto, *Adv. Mater.*, 2007, **19**, 3480-3484.

S7 C. Li, Y. Xue, M. Han, L. C. Palmer, J. A. Rogers, Y. Huang and S. I. Stupp, *Matter*, 2021, **4**, 1377-1390.

S8 C. Li, A. Iscen, H. Sai, K. Sato, N. A. Sather, S. M. Chin, Z. Álvarez, L. C. Palmer, G. C. Schatz and S. I. Stupp, *Nat. Mater.*, 2020, **19**, 900-909.

S9 W. Francis, A. Dunne, C. Delaney, L. Florea and D. Diamond, *Sens. Actuator B-Chem.*, 2017, **250**, 608-616.

S10 Z. Sun, Y. Yamauchi, F. Araoka, Y. S. Kim, J. Bergueiro, Y. Ishida, Y. Ebina, T. Sasaki, T. Hikima and T. Aida, *Angew. Chem.-Int. Edit.*, 2018, **57**, 15772-15776.

S11 B. Wu, Y. Xue, I. Ali, H. Li, Y. Yang, X. Yang, W. Lu, Y. Zheng and T. Chen, *Research*, 2022, **2022**, 0015.

S12 H. Arora, R. Malik, L. Yeghiazarian, C. Cohen and U. Wiesner, *J. Polym. Sci. Pol. Chem.*, 2009, **47**, 5027-5033.

S13 F. Vernerey and T. Shen, *J. R. Soc. Interface*, 2017, **14**, 20170242.

Table S2 Recipe for the preparation of aqueous solutions of copolymers by polymerization at room temperature.

Materials	**AAc** (g)	**AAm** (g)	**NIPAm** (g)	**KPS** (g)	**TEMED** (μL)	**AuNR** （nM)[a]	**H_2O** (mL)
P(AAc-*co*-AAm)	0.2	1.8	0	0.02	100	0	17.1
P(AAc-*co*-NIPAm)	0.3	0	1.8	0.02	100	3/5/10	12.9

[a] The nM (i.e., nmol/L) represents the content of AuNR in water.

Table S3 Printing parameters for the fabrication of hydrogel composites with aqueous solutions of copolymers and their mixture as the inks for passive, transtion, and active layers. Printing hydrogels are performed at room temperature.

Printing layers	**Printing ink**	**Nozzle moving speed** (mm/s)	**Extrusion pressure** (kPa)	**Nozzle diameter** (mm)
Passive layer	P(AAc-*co*-AAm) solution	7	396	0.19
Transition layer	Hybrid solution f_h = 50% [a]	7	396	0.19
Active layer	P(AAc-*co*-NIPAm) solution	7	396	0.19

[a] The volume ratio of P(AAc-*co*-NIPAm) in the mixture of P(AAc-*co*-NIPAm) and P(AAc-*co*-AAm) solutions.

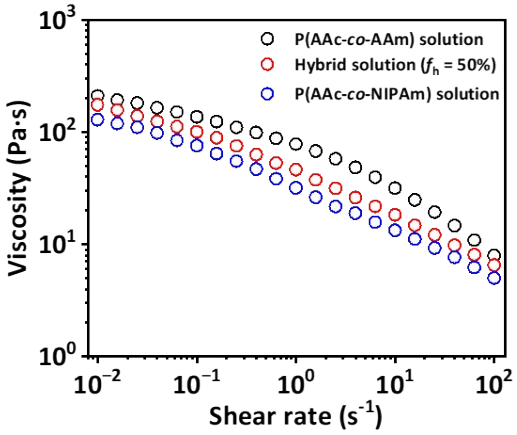

Fig. S1 Viscosity of the aqueous solutions of the copolymers and their mixture as a function of shear rate at room temperature. f_h is the volume ratio of P(AAc-*co*-NIPAm) in the mixture of P(AAc-*co*-NIPAm) and P(AAc-*co*-AAm) solutions. Steady shear measurements were performed to the solutions at room temperature. These solutions are used as the printing inks to fabricate gel fibers as the passive, transition, and active layers of the printed tough gels.

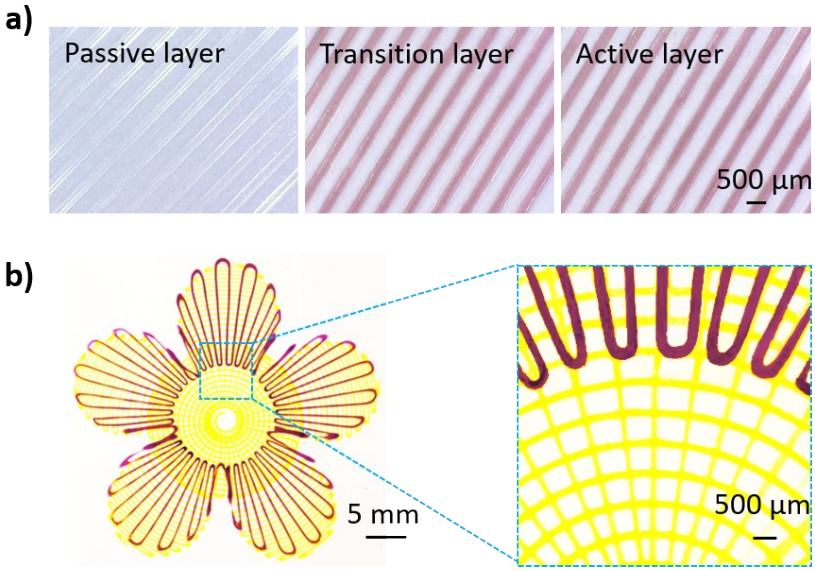

Fig. S2 Feature size of gel fibers and printed construct. (a) The printed gel construct consists of transparent passive layer, brown transition layer, and brown active layer. (b) Digital photos of the printed flower-like hydrogel. The structure contains four layers. The passive grid at the bottom of the printed structure is stained with quinoline yellow for better visualization. The transition and active layers are printed with the same arrangement and have a brown color due to the presence of AuNRs.

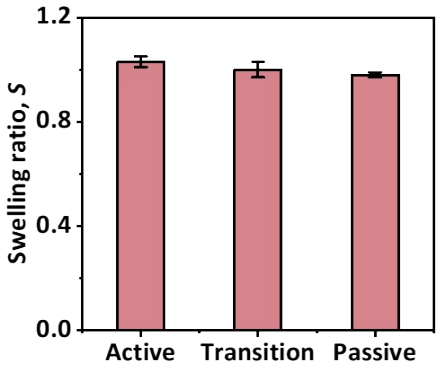

Fig. S3 Swelling ratio in length, *S*, of the printed active, transition, and passive gel fibers after being soaked in 0.1 M Zr^{4+} ion solution and then in pure water.

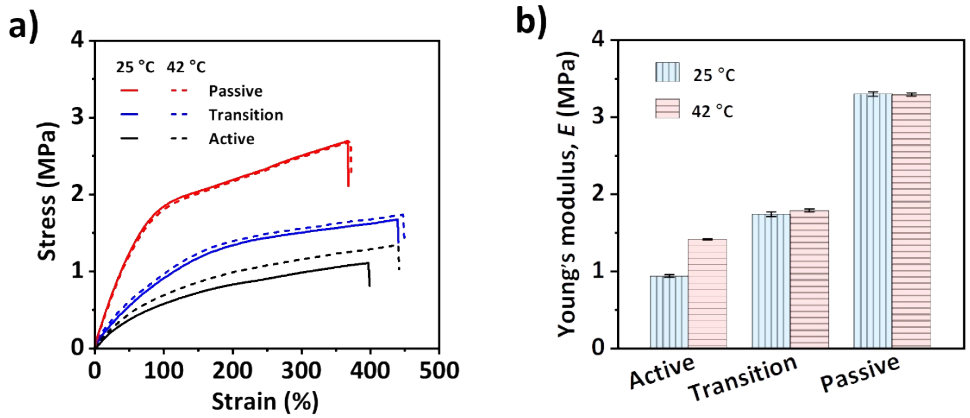

Fig. S4 Tensile stress-strain curves (a) and corresponding Young's moduli (b) of the active, transition, and passive gel fibers at 25 °C and 42 °C. Tensile tests are performed with the stretch rate of 100 mm/min.

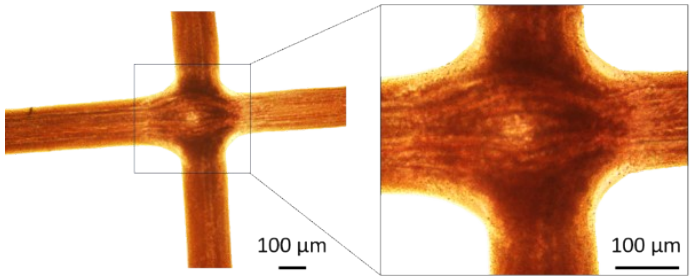

Fig. S5 Microscope images to show the contact area of the printed gel fibers. The bonding area between gel fibers is difficult to measure.

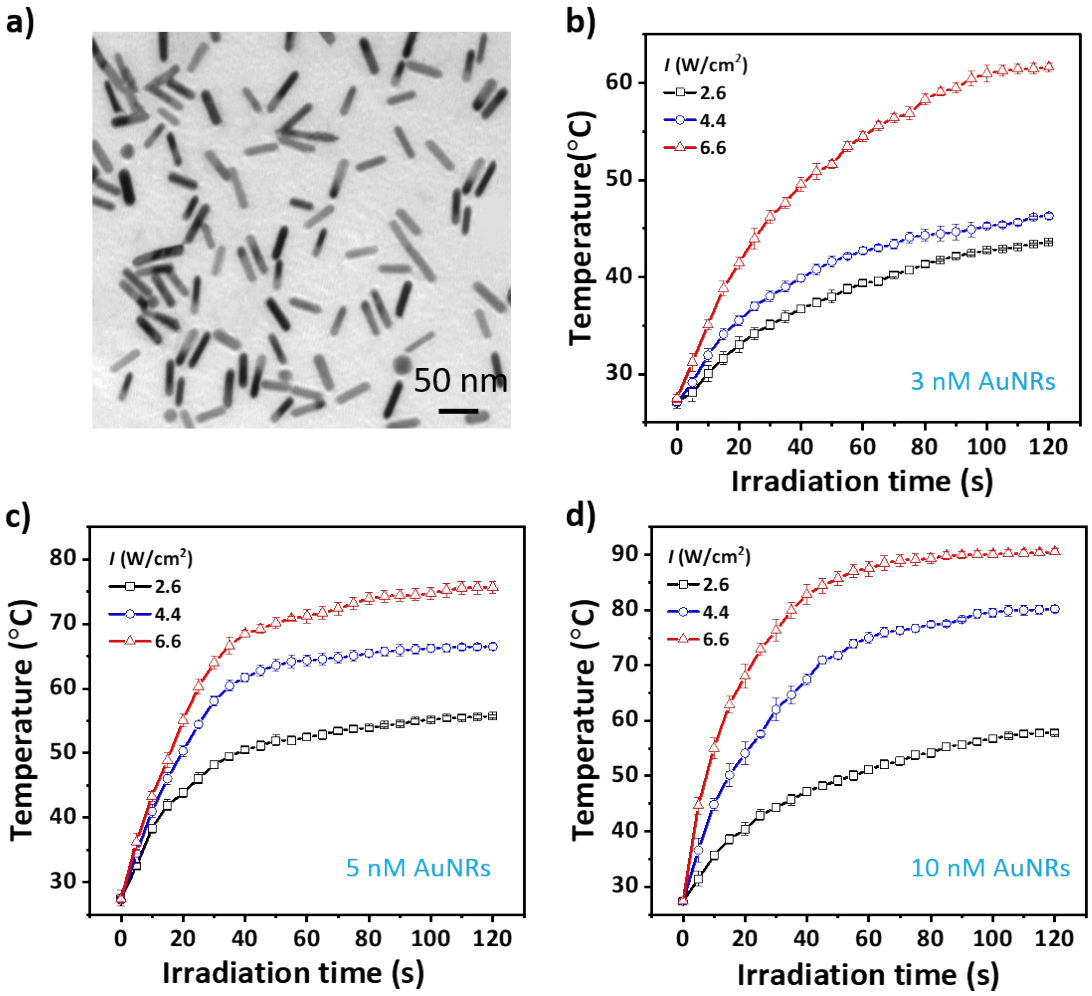

Fig. S6 Photothermal behaviors of AuNR suspensions and printed gels. (a) TEM image of the AuNRs. (b-d) Varying temperature of the printed tough hydrogel containing 3 nM (b), 5 nM (c), and 10 nM (d) AuNRs as a function of the irradiation time of NIR light with different power intensities, *I*.

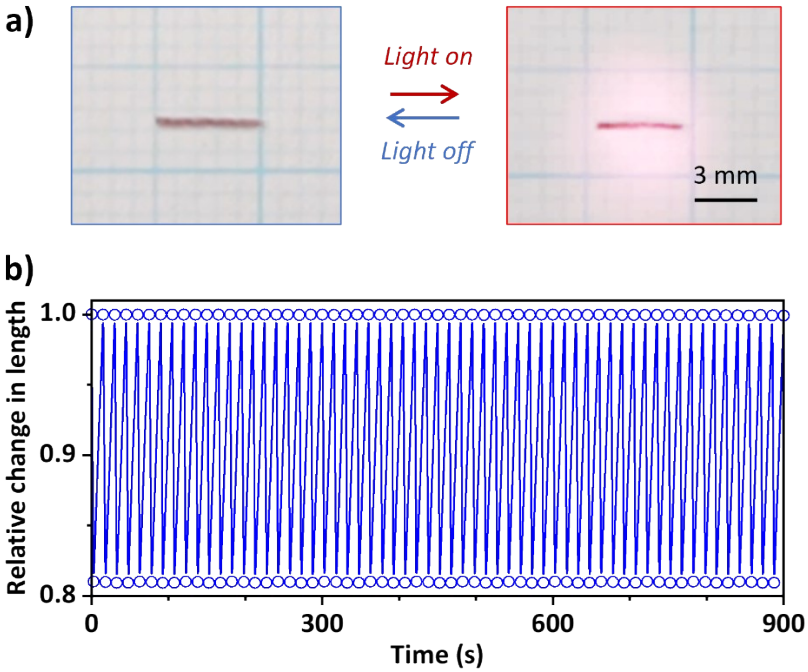

Fig. S7 Digital photos (a) and varying length of the active gel fiber (b) under cyclic NIR light irradiation with the intensity of 6.6 W/cm^2 for at least 60 times.

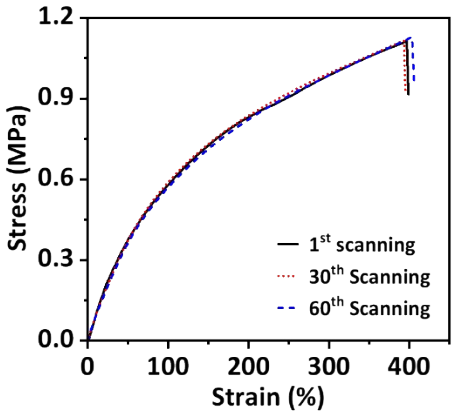

Fig. S8 Tensile stress-strain curves of the active gel fiber at room temperature after cyclic light irradiation for different times. The tensile tests are performed to the gel after the shape and properties recover their original state.

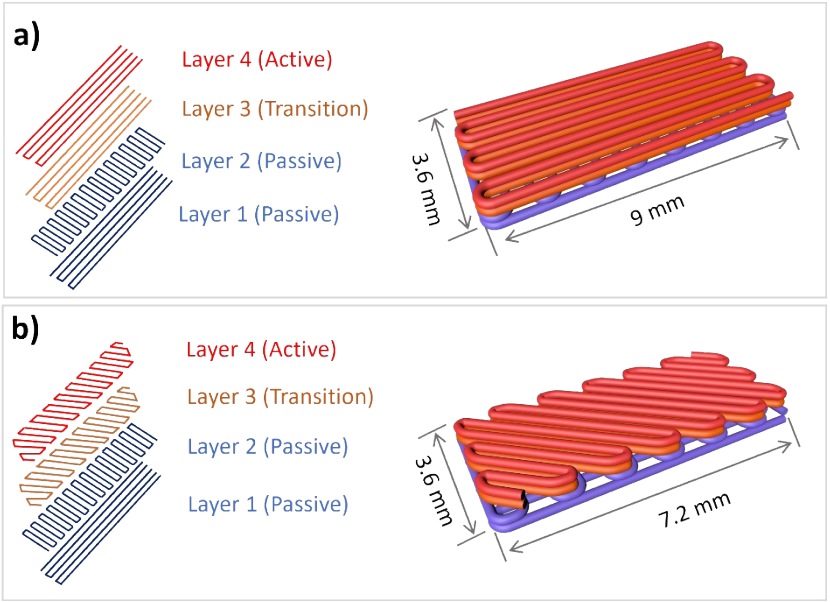

Fig. S9 Structure and dimensions of the printed gel in Fig. 3. The left is the schematic for the printing path of different tough gels as the passive, transition, and active layers of the gel. The right is the structure and dimensions of the printed four-layer hydrogel composites. The fibers in the transition and active layers (i.e. the third and fourth layers) are oriented at an angle of 0° (a) and 45° (b) with respect to the long axis of the printed constructs.

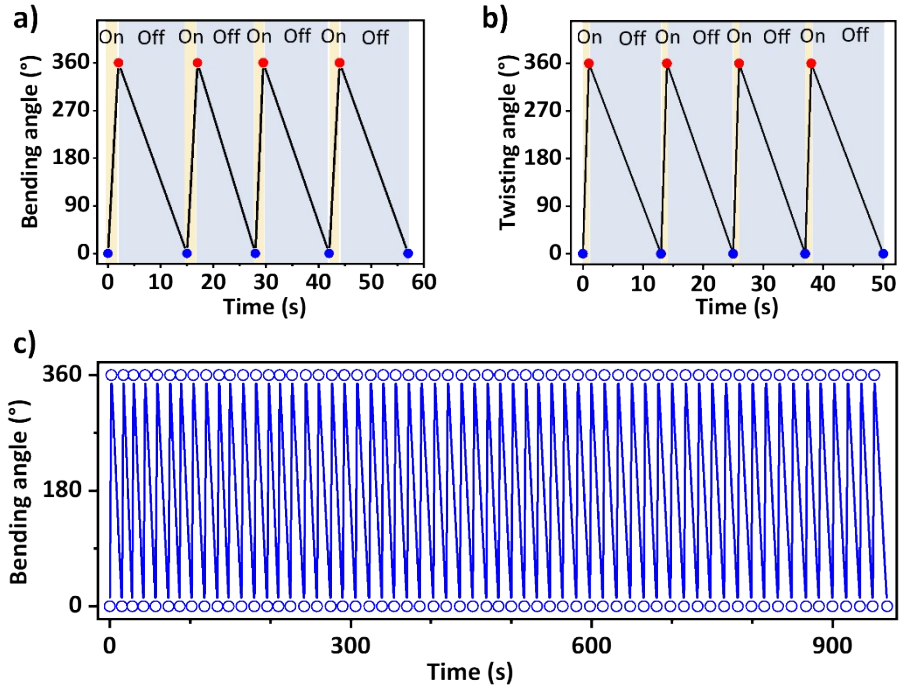

Fig. S10 Reversible bending of the printed gels under cyclic light irradiation. (a,b) Variations of instantaneous bending angle (a) and twisting angle (b) of the printed gels to form a roll and a cylinder helix, respectively, under cyclic scanning of a light spot at room temperature. The reversible deformations of the printed gels are shown in Figure 3e and 3f. (c) Reversible bending of the printed gel under cyclic light irradiation for at least 60 times.

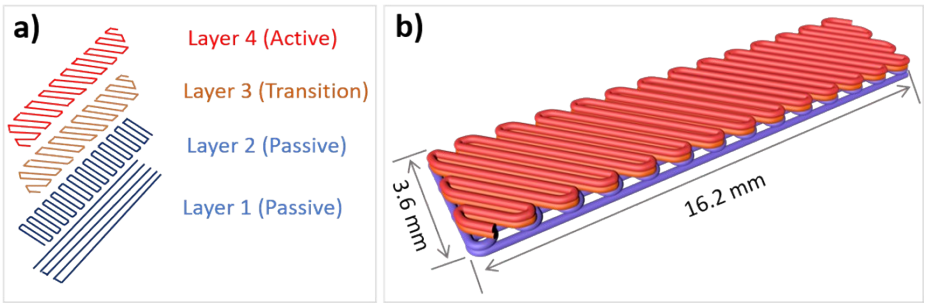

Fig. S11 Structure and dimensions of the printed gel in Fig. 4. (a) Schematic for the printing path of different tough gels as the passive, transition, and active layers of the gel robot. (b) Structure and dimensions of the printed tough gel as the soft roots with rotation and flipping motions under scanning light irradiation. The dynamic deformations and motions of the printed gel are shown in Figure 4.

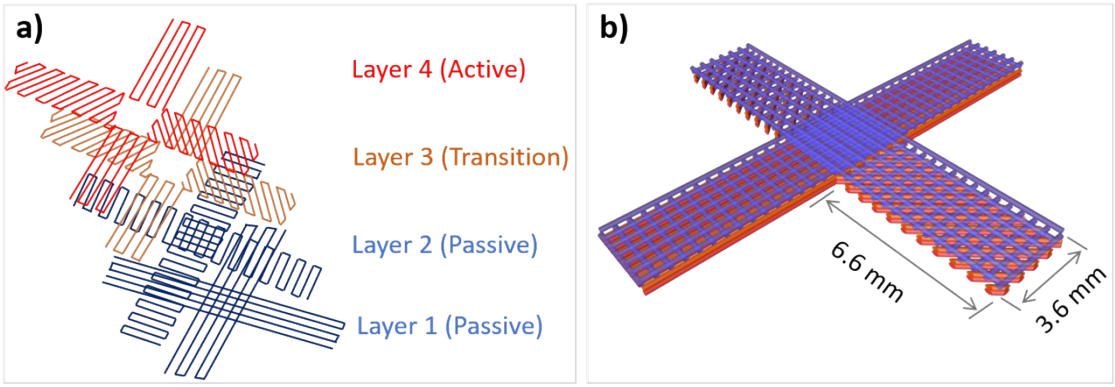

Fig. S12 Structure and dimensions of the gel in Fig. 5. (a) Schematic for the printing path of different tough gels as the passive, transition, and active layers of the modular gel robots. (b) Structure and dimensions of the printed four-footed hydrogel robot.

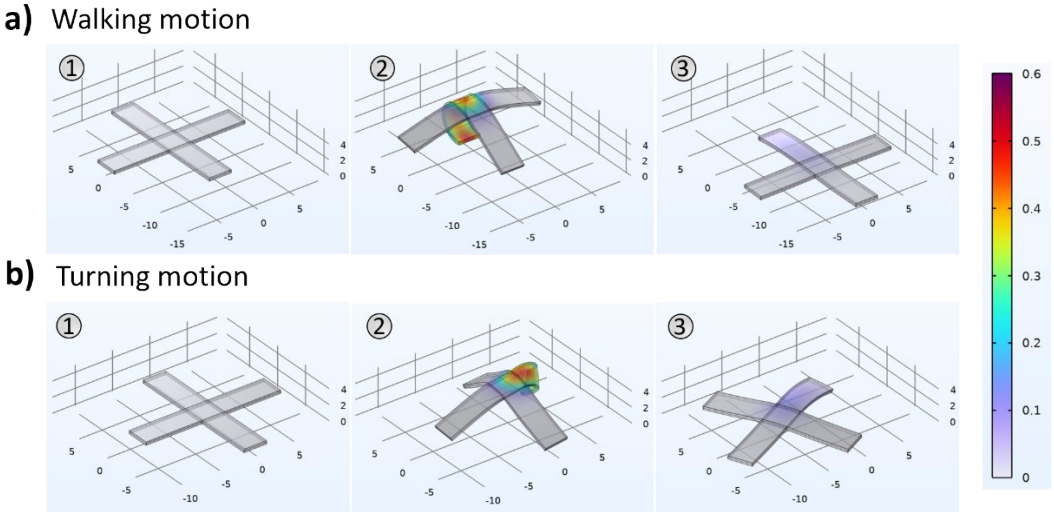

Fig. S13 Numerical simulations of the walking (a) and turning (b) motions of the printed modular gel under scanning light. Color scale indicates the normalized temperature.

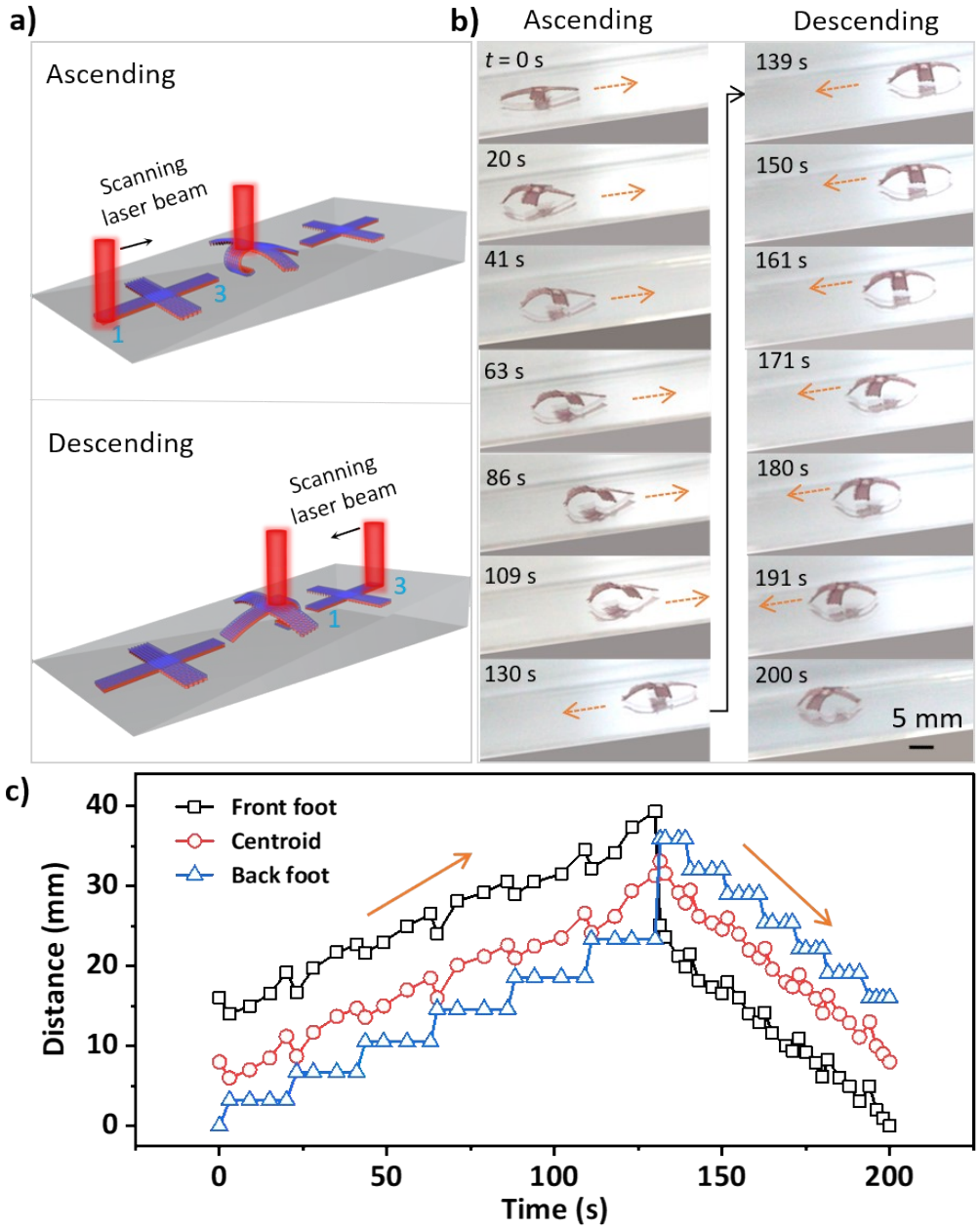

Fig. S14 Walking motions of the printed gel robot on an inclined substrate upon cyclic light irradiation. (a) Schematic for the light-steering ascending and descending of the printed hydrogel by scanning walking foot 1 and 3. (b) Serial photos to show the ascending (left column) and descending (right column) of the printed hydrogel on a glass substrate with an inclined angle of 8° under cyclic scanning of NIR light on the walking foot. The locomotion time, *t*, is shown in the photos. In each cycle, it takes around 21.66 s to take one step with about 3.88 mm during ascent, while it only takes around 10.16 s to take one step with about 4.18 mm during descent. (c) Displacements of the centroid, as well as the front and back feet, of the printed hydrogel as a function of the time under cyclic irradiation of scanning light.

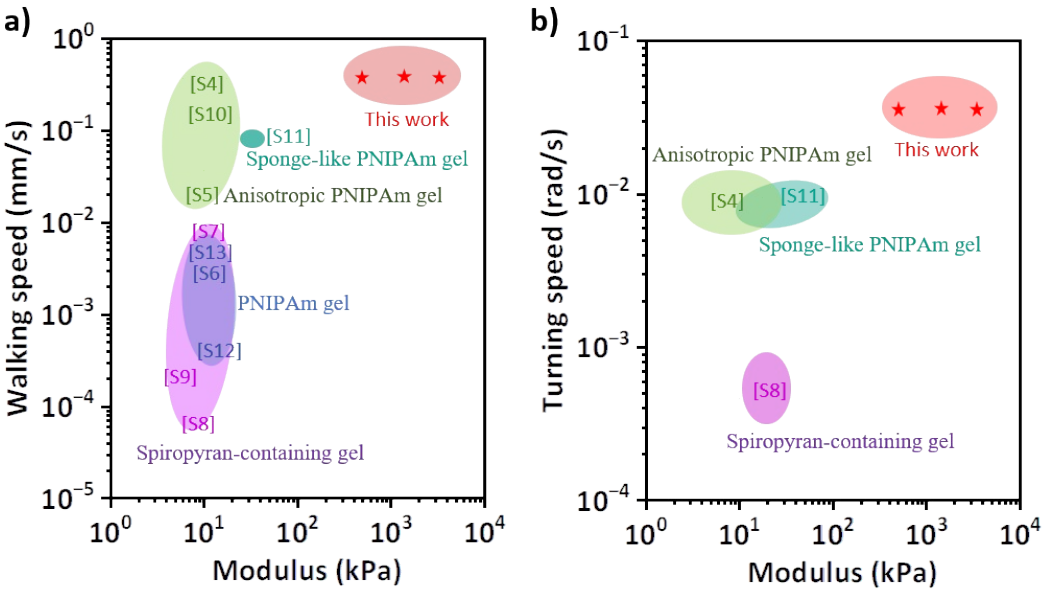

Fig. S15 Comparison of the robotic performances of various hydrogel-based soft robots. Walking speeds and turning speeds of various hydrogel robots with different elastic modulus upon cyclic heating or light irradiation.[S4-13]

References

S4 Q. L. Zhu, C. Du, Y. Dai, M. Daab, M. Matejdes, J. Breu, W. Hong, Q. Zheng and Z. L. Wu, *Nat. Commun.*, 2020, **11**, 5166.

S5 Y. S. Kim, M. Liu, Y. Ishida, Y. Ebina, M. Osada, T. Sasaki, T. Hikima, M. Takata and T. Aida, *Nat. Mater.*, 2015, **14**, 1002-1007.

S6 S. Maeda, Y. Hara, T. Sakai, R. Yoshida and S. Hashimoto, *Adv. Mater.*, 2007, **19**, 3480-3484.

S7 C. Li, Y. Xue, M. Han, L. C. Palmer, J. A. Rogers, Y. Huang and S. I. Stupp, *Matter*, 2021, **4**, 1377-1390.

S8 C. Li, A. Iscen, H. Sai, K. Sato, N. A. Sather, S. M. Chin, Z. Álvarez, L. C. Palmer, G. C. Schatz and S. I. Stupp, *Nat. Mater.*, 2020, **19**, 900-909.

S9 W. Francis, A. Dunne, C. Delaney, L. Florea and D. Diamond, *Sens. Actuator B-Chem.*, 2017, **250**, 608-616.

S10 Z. Sun, Y. Yamauchi, F. Araoka, Y. S. Kim, J. Bergueiro, Y. Ishida, Y. Ebina, T. Sasaki, T. Hikima and T. Aida, *Angew. Chem.-Int. Edit.*, 2018, **57**, 15772-15776.

S11 B. Wu, Y. Xue, I. Ali, H. Li, Y. Yang, X. Yang, W. Lu, Y. Zheng and T. Chen, *Research*, 2022, **2022**, 0015.

S12 H. Arora, R. Malik, L. Yeghiazarian, C. Cohen and U. Wiesner, *J. Polym. Sci. Pol. Chem.*, 2009, **47**, 5027-5033.

S13 F. Vernerey and T. Shen, *J. R. Soc. Interface*, 2017, **14**, 20170242.

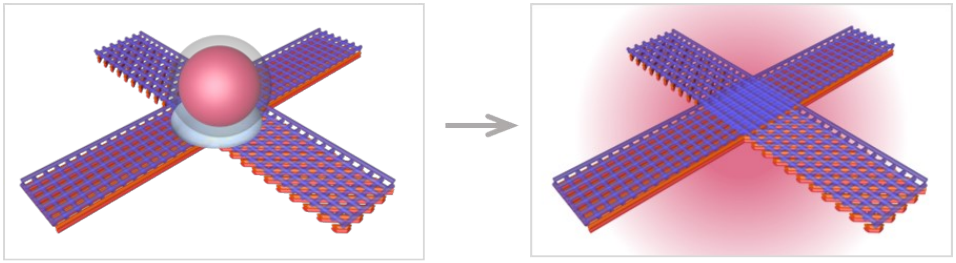

Fig. S16 Schematic for the design of printed hydrogel robot for cargo transportation. A gelatin gel ball loaded with dye molecules is adhered to the center of the printed hydrogel robot. This cargo is released at the destination by laser irradiation on the gel ball that results in localized heating and thus melting of the gelatin gel ball and release of the dye molecules. The masses of gelatin ball and printed hydrogel are 0.08 g and 0.015 g, respectively.

Legends of supplementary videos

Movie S1. Reversible rolling of the printed hydrogel strip under cyclic light irradiation.

Movie S2. Reversible twisting of the printed hydrogel strip under cyclic light irradiation.

Movie S3. Dynamic twisting and flipping of the hydrogel strip under cyclic light irradiation.

Movie S4. Light-steered walking and tuning motions of the four-footed hydrogel robot on a glass substrate under cyclic light irradiation.

Movie S5. Numerical simulation showing the walking motion of the hydrogel robot under scanning light stimulation.

Movie S6. Numerical simulation showing the turning motion of the hydrogel robot under scanning light stimulation.

Movie S7. Photo-steered multi-gait locomotion of the printed four-footed hydrogel robot to cross the maze and transport a cargo to the destination.